JOURNAL OF GEOPHYSICAL RESEARCH, VOL. 110, D21315, doi:10.1029/2005JD006127, 2005

Isotopomer fractionation in the UV photolysis of N_2O: Comparison of theory and experiment

Meher K. Prakash, Jason D. Weibel,[1] and R. A. Marcus
Noyes Laboratory of Chemical Physics, California Institute of Technology, Pasadena, California, USA

Received 24 April 2005; accepted 18 August 2005; published 12 November 2005.

[1] In the photodissociation of N_2O, absorption cross sections differ with isotopic substitution, leading to a wavelength-dependent fractionation of the various isotopomers. Several models ranging from shifts by zero-point energy differences to propagation of wave packets on the excited electronic state potential energy surface have been proposed to explain the observed fractionations. We present time-independent fractionation calculations for the isotopomers 447, 448, 456, 546, and 556. Besides largely agreeing with the experimental data, these calculations have the advantage of not being computationally intensive, as well as satisfying the physical facts that the asymmetric stretch and the doubly degenerate bending vibration are the principal Franck-Condon active modes in the photodissociation. The latter is reflected in the actual dissociation and in the high rotational excitation and lack of vibrational excitation of the N_2 product. The calculations are based on a multidimensional reflection principle using an ab initio potential energy surface. The theory for the absorption cross section and isotopomer fractionation accompanying photodissociation is described. The absolute value of the theoretically calculated absorption cross section is very close (90%) to the experimentally observed value. The present computations also provide data for the slope of a three-isotope plot of the fractionation of 447/446 relative to 448/446, using the fractionations at different wavelengths. The resulting slope is compared with a perturbation theoretical expression for direct photodissociation given elsewhere.

Citation: Prakash, M. K., J. D. Weibel, and R. A. Marcus (2005), Isotopomer fractionation in the UV photolysis of N_2O: Comparison of theory and experiment, *J. Geophys. Res.*, *110*, D21315, doi:10.1029/2005JD006127.

1. Introduction

[2] Nitrous oxide (N_2O) is an efficient greenhouse gas and a source of singlet oxygen. Even though its concentration in the atmosphere is about 3 orders of magnitude less than that of CO_2, it gains its importance because its per molecule global warming potential is about 200–300 times that of CO_2 [*Yung et al.*,1976]. Isotopomer fractionation measurements are important in determining sources and sinks of atmospheric gases [*Stevens et al.*, 1972; *Brenninkmeijer et al.*, 2003]. The sources and sinks and the isotopic behavior of N_2O have been the subject of many studies [*Kim and Craig*, 1993; *Naqvi et al.*, 1998; *Brenninkmeijer et al.*, 2003], because of the atmospheric importance of N_2O. In the atmosphere there are two main pathways for removal of N_2O, photolysis and photo-oxidation by $O(^1D)$:

$$N_2O + \hbar\omega \rightarrow N_2(^1\Sigma^+) + O(^1D) \quad (1)$$

$$N_2O + O(^1D) \rightarrow N_2 + O_2 \text{ or } 2NO \quad (2)$$

[3] Although a photo-dissociation can also yield triplet oxygen $O(^3P)$, this reaction has a negligible quantum yield [*Preston and Barr*, 1971], compared to the quantum yield of Reaction (1) that is nearly unity [*Preston and Barr*, 1971; *Atkinson et al.*, 1997, and references therein]. The quantum yield of the triplet formation was recently measured [*Nishida et al.*, 2004] to be about 0.5%. Reactions (1) and (2) form the principal means of N_2O dissociation in the stratosphere, with contributions of about 90% and 10%, respectively [*Minschwaner et al.*, 1993]. The absorption in N_2O is peaked at around 182 nm and is dominated by a singlet-singlet transition [*Brown et al.*, 1999]. The transition dipole moment for the particular transition is zero when the molecule is linear, and so the transition is electronic dipole forbidden. The transition, however, becomes allowed when the molecule deviates from linearity.

[4] *Selwyn and Johnston* [1981] measured the ultraviolet absorption cross sections of various isotopomers of N_2O over the wavelength range 172 to 197 nm and between 150 K and 500 K. In the analysis of their data, they concluded that the temperature dependence of the absorption spectrum is due to the thermal activation of the bending mode. Further, no rotational structure was observed in their measurements. Several authors have performed laboratory experiments to study the relative absorption cross sections/photolysis rates of various isotopomers [*Johnston et*

[1]Now at Division of Geological and Planetary Sciences, California Institute of Technology, Pasadena, California, USA.

0148-0227/05/2005JD006127

al., 1995; *Zhang et al.*, 2000; *von Hessberg et al.*, 2004, and references therein]. Atmospheric observations have been made to obtain the relative abundances of various isotopomers of N_2O [*Kim and Craig*, 1993; *Rahn and Wahlen*, 1997; *Park et al.*, 2004, and references therein]. *Prasad* [1997] proposed the possibility of new atmospheric sources of N_2O to account for the isotopomer fractionations. *Yung and Miller* [1997] explained the lack of isotopomer enrichment in N_2O at 185 nm [*Johnston et al.*, 1995] by introducing a model for isotopomer fractionation that varied with absorption wavelength. In their model, isotopomer fractionation was calculated on the basis of changes in the wavelength-dependent isotopomer optical absorption cross section due to differences in the zero-point energy (ZPE) of the isotopomers. While this model could provide only qualitative agreement with the experimental results, it motivated many wavelength-dependent fractionation measurements [*Turatti et al.*, 2000; *Zhang et al.*, 2000; *Kaiser et al.*, 2003; *von Hessberg et al.*, 2004].

[5] After this 1997 advance, efforts were made to bring the model into closer agreement with experimental measurements, and a time-dependent quantum mechanical calculation was made [*Johnson et al.*, 2001] on the basis of ab initio potential energy surfaces obtained by *Brown et al.* [1999] and using a propagated wave packet. The inclusion of the details of the potential energy and dipole moment surfaces into the analysis was a significant improvement. The results of their insightful work do not provide a full explanation of the experimental results (compare figures given later). One possibility, as indicated in the normalization constant used for the ground vibrational state in their equation (10) and confirmed by private communication (M. S. Johnson, private communication, April 2005), was that the two-dimensional (2-D) nature of the bending vibration was treated as a bending in a plane for calculating bending mode wave functions, and then treating the 2-D aspect only by a degeneracy factor. The 2-D bending vibrational wave functions differ from those for a single bending vibration in a plane. Using the present calculational method, the effect of using a single bending mode method as a substitute for the 2-D one is given later in section 4.

[6] In the experiments of *Kaiser et al.* [2003], a depletion of some heavier isotopomers at 185 nm was recorded for the first time, while *Johnson et al.* [2001] predict enrichment or near-zero fractionation. *Blake et al.* [2003] achieved good results for the fractionation of 448 by adding a new feature to the ZPE model: the zero-point energy of the isotopomer affects not only the position of the absorption cross section but also the width. They fitted the absorption spectrum to a Gaussian form to extract the parameters for the most abundant isotopomer, 446. *Liang et al.* [2004], continued in a similar direction but they assumed, instead, that the ZPE contribution was from the two stretching modes rather than from all the modes, presumably because it yielded good results even for 546.

[7] However, the actual experiment-based physics of the dissociation show that the two stretching modes play a very different role from each other, and the bending modes also play a very important role: *Hanisco and Kummel* [1993] showed that the photodissociation of N_2O yields vibrationally cold (about 98% of dissociated N_2 is in the $\nu'' = 0$ state) and rotationally hot ($J = 74$) molecular nitrogen. Upon excitation to the higher electronic state, the N-O stretching mode becomes a repulsion and leads to a dissociation, while the N-N is not significantly excited. So, treating the two stretching modes on the same basis and excluding the bending is at odds with these observations.

[8] Recently, *von Hessberg et al.* [2004] have published high-precision cross-section measurements of 456, 546 and 556, over a wavelength range 181 nm to 218 nm at 233 K and 283 K. The fractionation values computed from these cross-section measurements form an extensive set of data that can help in understanding the atmospheric measurements. *Nanbu and Johnson* [2004] have removed a restriction present in the earlier ab initio calculations by calculating the full three-coordinate potential energy surface and using it for the cross-section and isotopomer fractionation computations. The wave functions used in this paper for forming the wave packet are the 2-D bending ones (M. S. Johnson, private communication, April 2005).

[9] In the present article, a time-independent multidimensional reflection principle is used for the calculation of the absorption cross sections of the N_2O isotopomers and there by the fractionations of the heavy isotopomers relative to the 446. This method, described in section 2, focuses on the envelope of the absorption cross section rather than on the weak superimposed structure. We use the experimental force constant data to calculate the normal mode frequencies of the N_2O molecules in their initial vibrational state and hence calculate the wave functions. We use the ab initio potential energy surfaces calculated by *Daud et al.* [2005]. These potential energy surfaces depend on two coordinates, like the ones given by *Brown et al.* [1999]. Experimentally, the N-N bond distance changes by only 3% during dissociation and was assumed constant in these two coordinate potential energy surface calculations. *Nanbu and Johnson* [2004] have relaxed this restriction of keeping N-N bond fixed. However, their potential energy surface data have not been published as yet and we have used the latest surfaces published by *Daud et al.* [2005].

[10] The article is organized as follows: The theory is presented in section 2, the detailed procedure for the present calculations in section 3, the results are presented and discussed in section 4 and conclusions are drawn in section 5.

2. Theory

[11] Photodissociation is classified as indirect (or predissociation) or direct. In the latter, the parent molecule dissociates immediately upon excitation to the upper electronic state. In indirect photofragmentation a potential barrier hinders direct fragmentation of the excited complex and the wave packet spends a finite lifetime in the local potential energy well before dissociating. Direct dissociation is characterized by a diffuse, almost structureless absorption spectrum. A comparison among the absorption cross sections of bands corresponding to direct, nearly direct and indirect dissociations can be found in Figure 1.6 of *Schinke* [1993]. In the case of N_2O, the broad envelope, with a superimposed weak structure, indicates that the dissociation proceeds primarily in a direct way. We are interested in the envelope of the absorption cross section, and calculate the energies absorbed in a vertical transition

from electronic ground to excited state. This procedure automatically includes the contribution due to the partial absorption cross sections corresponding to various quantum states of dissociating molecule. The formal theory for this behavior for multidimensional systems is due to *Heller* [1978] and an early version is described by *Schinke* [1993]. It is summarized here, together with a more accurate version given by *Lee et al.* [1983].

2.1. Absorption Cross Section

[12] The molecular quantum states are given in terms of all electronic (**X**) and nuclear (**R**) coordinates. We consider the transition of the molecule from the initial molecular quantum state **I**, with energy E_I, to a final quantum state **F**, with energy E_F. The absorption cross section, $\sigma_{FI}(\omega)$, for an allowed transition is given in terms of the electric dipole operator **d** of the molecule as in equation (3), an example of Fermi's Golden rule.

$$\sigma_{FI}(\omega) = \frac{\pi}{\hbar\epsilon_0 c}\ \omega\ \delta\left(\omega_{F,I} - \omega\right)\ |\langle \mathbf{F}|\mathbf{e}.\mathbf{d}|\mathbf{I}\rangle|^2 \tag{3}$$

where $\omega_{F,I} = (E_F - E_I)/\hbar$ is the corresponding 'transition frequency', **e** is a unit vector in the direction of the polarization of the electric field and $|\langle \mathbf{F}|\mathbf{e}.\mathbf{d}|\mathbf{I}\rangle|$ is the matrix element for the transition from the initial to the final states. Equation (3) is applicable equally to bound-bound, bound-free and free-free transitions and is the key equation for the time-independent photodissociation for spin-allowed, dipole-allowed transitions.

[13] To compute the absorption cross section in the present case, the Born-Oppenheimer approximation is introduced, so separating the molecular wave function into a nuclear part $\Psi(\mathbf{R})$ and an electronic part $\Phi(\mathbf{X};\ \mathbf{R})$. The electronic wave function will be indexed by i, f and the nuclear wave function by ν, ν', respectively, corresponding to the initial and final states.

[14] The absorption cross section $\sigma_{i\nu}(\omega)$ for transition from the initial electronic and vibrational (vibronic) state (i, ν), to the possibly degenerate final vibronic states (f, ν') is given as:

$$\begin{aligned}\sigma_{i\nu}(\omega) &= \frac{\pi}{\hbar\epsilon_0 c}\sum_{\nu'}\omega\ \delta\left(\omega_{f\nu',i\nu} - \omega\right)\ |\langle\Psi_{\nu'}|\langle\Phi_f|\mathbf{e}.\mathbf{d}|\Phi_i\rangle|\Psi_\nu\rangle|^2 \\ &= \frac{\pi}{\hbar\epsilon_0 c}\sum_{\nu'}\omega\ \delta\left(\omega_{f\nu',i\nu} - \omega\right)\ |\langle\Psi_{\nu'}|\mathbf{e}.\boldsymbol{\mu}_{fi}|\Psi_\nu\rangle|^2\end{aligned} \tag{4}$$

where $\boldsymbol{\mu}_{fi} = \langle\Phi_f|\mathbf{d}|\Phi_i\rangle$ is the transition dipole moment, $\omega_{f\nu',i\nu} = (E_{f\nu'} - E_{i\nu})/\hbar$ and the sum is over the nuclear vibrational states ν' in the given final electronic state f. When the initial state ν is degenerate, one sums $\sigma_{i\nu}$ over the degenerate states ν.

[15] The above expression for the absorption cross section is in the time-independent form, and its calculation requires a knowledge of the nuclear wave functions in the upper electronic state. The calculation of the wave functions in the excited electronic state would normally be complicated, unlike that of the ground electronic state vibrational wave functions which can be found easily using a harmonic oscillator approximation for the vibrational potential energy. To circumvent this problem, we use a Franck-Condon type approximation, which is more easily seen in the time-dependent form [*Lee*, 1982; *Lee et al.*, 1983]. Using the details sketched in Appendix A, one obtains the expression for the absorption cross section as:

$$\sigma_{i\nu} = \frac{\pi\omega}{3\hbar\epsilon_0 c}\int |\Psi_\nu(\mathbf{R})|^2 \left|\mu_{fi}(\mathbf{R})\right|^2 \delta\left(\omega - \left(V_f(\mathbf{R}) - \frac{1}{2}E_{i\nu}\right)/\hbar\right) d\mathbf{R} \tag{5}$$

where μ_{fi} is the magnitude of the vector $\boldsymbol{\mu}_{fi}$ and $V_f(\mathbf{R})$ is the potential energy of the excited state and $E_{i\nu}$ is the average vibrational energy in the ground electronic state and (1/2) $E_{i\nu}$ is the average potential energy for the case of a harmonic oscillator.

[16] In this final form for the absorption cross section only the excited state potential surface, transition dipole moment surface, and the probability density in the ground electronic state are needed to calculate the absorption cross section. The wave functions in the excited electronic state are not needed. A reflection principle for the one-vibration coordinate case was used by *Winans and Steuckelberg* [1928] and is also given by *Herzberg* [1950]. It was generalized by *Heller* [1978] for the multidimensional case. However, in that expression, at the vibrational turning point the kinetic energy in the direction of steepest descent as well as normal to it was taken to be zero. This approximation was corrected later by *Lee et al.* [1983] and our equation (5) is this corrected form of multidimensional reflection principle. In the present case the **R** in equation (5) denotes the internal coordinates for the asymmetric stretching vibration and the doubly degenerate bending vibration.

[17] According to equation (5), the absorption at any frequency, ω, is proportional to the probability that the initial state is at a **R** for which the vertical transition, given by the delta function in equation (5), is equal to the potential energy of the electronically excited state at **R** minus an average potential energy $(1/2)E_{i\nu}$, in the lower electronic vibrational state. Equation (5) is implemented in section 4 to calculate the absorption cross section from each vibrational level in the ground electronic state and then the total absorption cross section $\sigma(\omega)$ by using the thermal population as a weight.

2.2. Enrichment

[18] Different isotopomers have the same potential energy function but differ in their normal mode frequencies and normal coordinates, and hence have different widths of the electronic ground state wave functions. As such, they have different absorption cross sections $\sigma_{i\nu}(\omega)$, resulting in a wavelength-dependent fractionation of isotopomers. Once the absorption cross sections for various isotopomers are calculated, the fractionation of the different isotopomers relative to the most common isotopomer can be found. The photodissociation rate $J(\omega)$ of a single molecule is given in terms of an absorption cross section $\sigma_{total}(\omega)$ calculated from $\sigma_{i\nu}$'s (equation (9)) as

$$J(\omega) = \sigma_{total}(\omega)\ I(\omega)\phi(\omega) \tag{6}$$

where $I(\omega)$ is the photon flux and $\phi(\omega)$ is the quantum yield at energy, $\hbar\omega$. The fractionation $\epsilon(\omega)$ of one isotopomer

relative to another due to a one-step photolysis reaction can be defined as the ratio of photodissociation rates,

$$\epsilon(\omega) = \frac{J'(\omega)}{J(\omega)} - 1 = \frac{\sigma'_{total}(\omega)\phi'(\omega)}{\sigma_{total}(\omega)\phi(\omega)} - 1 = \frac{\sigma'_{total}(\omega)}{\sigma_{total}(\omega)} - 1 \qquad (7)$$

where the last equality ($\phi'(\omega) = \phi(\omega) = 1$) holds when the upper state is purely dissociative with no singlet-triplet intersystem crossing in the dissociative state (Triplet-singlet spin forbidden transitions are enhanced by nuclear spin–electron spin coupling (''hyperfine interactions'') when one of the nuclei has a nonzero nuclear spin).

3. Procedure

[19] The isotope effects enter into the calculation only through the ground electronic state vibrational wave functions and the energy $E_{i\nu}$. The potential energy surfaces and dipole moment function expressed in mass-independent internal coordinates are independent of isotopic substitution. The results of the potential energy and dipole moment surface calculations by *Daud et al.* [2005] are given in terms of mass-dependent Jacobi coordinates and for the present use, they had to be re-expressed in terms of the internal coordinates (Appendix B).

[20] In its electronic ground state N_2O is a linear triatomic molecule and hence has four normal modes of vibration, the symmetric and asymmetric stretching modes and a doubly degenerate bending mode. As usual the wave functions for the ground electronic state is written in terms of the normal mode coordinates for these vibrations, and the total vibrational wave function is the product of the individual wave functions for each of the modes. In the normal coordinates the harmonic oscillator wave functions (for the asymmetric stretching and each of the two degenerate bending modes) are given in terms of the well known Hermite polynomials [*Cohen-Tannoudji et al.*, 1977]. The vibrational ground state wave function for the asymmetric stretching mode is given, for example, as $(\alpha^2/\pi)^{1/4}\ \exp(-\alpha^2 r^2/2)$, where α is a constant depending on normal mode frequencies, discussed in Appendix B and conversion factors from internal to normal coordinates, as discussed in Appendix C. Since the potential energy is dependent only upon the magnitude of a bending angle θ and not upon the angle ϕ about the linear axis, the wave functions for the two degenerate bending modes can be combined so that the integrand in equation (5) depends on wave functions as a function of θ and not of the azimuthal angle ϕ. The corresponding wave functions for such a case are given in terms of Laguerre polynomials [*Freed and Band*, 1977; *Cohen-Tannoudji et al.*, 1977]. For convenience, the first three wave functions for the degenerate bending vibrations are given in Table C1 in Appendix C.

[21] Once the total wave function is found in terms of the normal coordinates, using the relationship between the internal and normal coordinates, also given in Appendix B, the wave functions are converted into functions of internal coordinates. The procedure and data needed for this transformation are given there.

[22] For our calculations, the electronically excited state potential is approximated in the vicinity of the most probable initial spatial region by $V = V_e - V_1(r_{NO}) - V_2(\theta)$, where V_e is the difference of the potential energy of the excited electronic state from the average potential energy of ground electronic state, at the electronic ground state equilibrium position and (r_{NO}, θ) denote the deviations from the equilibrium internal coordinates (r_{NO}^{eq}, $\theta^{eq} = 0$) in the lower electronic state. $V_1(r_{NO})$ and $V_2(\theta)$ are the changes in potential energy as a function of the displacements r_{NO} and θ. In evaluating the $\sigma_{i\nu}$ given by equation (5), $\mathbf{R} = (r_{NO}, \theta)$ would thus be the relevant nuclear coordinates. The volume element for angles is $\sin\theta d\theta d\phi$. Given that the potential energy, dipole moment surfaces and $|\Psi_\nu|^2$ are independent of ϕ, the integration over ϕ yields 2π. Using the delta function in equation (5), an integration is first performed over the coordinate r_{NO}. This step results in the replacing of r_{NO} in the integrand by r_{NO}^s, where r_{NO}^s is the function of θ obtained by solving the equation $(1/2)E_{i\nu} + \hbar\omega = V_e - V_1(r_{NO}) - V_2(\theta)$, a cubic in r_{NO}. One obtains

$$\sigma_{i\nu}(\omega) = \frac{\pi\omega}{3\hbar\epsilon_0 c} 2\pi \int \frac{-1}{(\partial V_1(r_{NO})/\partial r_{NO})_{r_{NO}^s}} \cdot \left|\Psi_\nu(r_{NO}^s, \theta)\right|^2 \left|\mu_{fi}(r_{NO}^s, \theta)\right|^2 \sin\theta d\theta \qquad (8)$$

where the first term in the integrand appears because the argument of the δ function is not the integration variable r_{NO}, but a function of it. The integration over the coordinate θ was then performed numerically using Mathematica.

[23] The absorption cross section was thus obtained as a continuous function of ω because the transition from any vibrational state in the ground electronic state occurs to a continuum of states in the excited electronic state. If the transition were instead to a single state, the absorption cross section would be a line spectrum rather than a continuum. For r_{NN}, it was observed [*Hanisco and Kummel*, 1993], as noted earlier, that 98% of the dissociated N-N is formed in ground vibrational state. So, for the purpose of this work, we can assume that the transition is to the N-N ground vibrational state in the excited electronic state. The only effect of including this ground vibrational mode of N-N in the calculations is to shift the absorption cross section by the difference in zero-point energy of N-N in ground and excited electronic states. We need the excited state potential surface along the N-N coordinate to compute the N-N frequency and not for obtaining a ''reflection principle'' method based on that surface. To this end, we used *Hopper* [1984] since this information was not reported in a later publication of *Nanbu and Johnson* [2004]. Within the wavelengths of interest, the calculations differ from those based on a fixed N-N coordinate by a maximum of about 10 per mil for 556 and 5 per mil for the other isotopomers.

[24] *Selwyn and Johnston* [1981] discuss the importance of the bending mode. In the analysis of their data they concluded that the temperature dependence of the absorption cross section is due to the excitation of the bending mode. To explore this point, we used the contributions to the absorption cross section calculated from the ground, first and second excited bending vibrational states denoted by [000], [010] and [020]. The stretching modes in this designation are in the vibrational ground

Table 1. Normal Mode Frequencies of the Isotopomers[a]

Isotopomer	ν_1	ν_2	ν_3
446	1284.903[b]	588.768[c]	2223.757[d]
446	1297.4	593.3	2280.5
447	1264.704[b]	586.362[e]	2220.074[d]
447	1274.8	590.8	2276.8
448	1246.885[b]	584.225[e]	2216.711[d]
448	1254.3	588.6	2273.7
456	1280.354[b]	575.434[c]	2177.657[d]
456	1295.6	579.7	2231.4
546	1269.892[b]	585.312[c]	2201.605[d]
546	1280.4	589.7	2257.8
556	1265.334[b]	571.894[e]	2154.726[d]
556	1279.0	576.1	2207.9

[a]Frequencies are given in cm^{-1}. For each isotopomer, lower row gives value from this work, and upper row gives experimental value.
[b]*Toth* [1986].
[c]*Jolma et al.* [1983].
[d]*Toth* [1987].
[e]*Amiot* [1976].

state. The total absorption cross section is given by the formula:

$$\sigma_{total}(T) = \frac{\sigma_{[000]} + \left(\sigma_{[01^{+1}0]} + \sigma_{[01^{-1}0]}\right)e^{\frac{-\hbar\omega_2}{k_BT}} + \left(\sigma_{[02^{+2}0]} + \sigma_{[02^{0}0]} + \sigma_{[02^{-2}0]}\right)e^{\frac{-2\hbar\omega_2}{k_BT}}}{1 + 2e^{\frac{-\hbar\omega_2}{k_BT}} + 3e^{\frac{-2\hbar\omega_2}{k_BT}}} \quad (9)$$

where $\omega_2 = 2\pi\nu_2$, with ν_2, as given in Table 1, is the frequency of the bending mode and the notation such as $[0n^{+l}0]$ is used for the degenerate or nearly degenerate states of [0n0], distinguished by a vibrational quantum number l that varies from $-n$ to n in increments of ±2 [*Freed and Band*, 1977]. The coefficients 1, 2, 3 in the denominator account for the degeneracy of the states [000], [010] and [020], respectively, in the thermal population. Although the energy of [100] mode is less than that of [020] mode, in our calculations, the contribution of [100] to the absorption cross section is less than 1% of the total absorption cross section at the same wavelength and we calculated that the difference it makes to fractionation calculations is less than 1 per mil. The reason for this low contribution is, besides the low thermal population of this nondegenerate mode, the low transition dipole moment, because the bending vibration is not in an the excited state in that thermal excitation. In the results presented in the next section, these small contributions from [100] state are omitted.

[25] *Selwyn and Johnston* [1981] attributed the weak structure in the absorption cross section to an effect of the bending vibrational state in the excited electronic state, although the origin of the weak structure is uncertain [*Nanbu and Johnson*, 2004; *Daud et al.*, 2005]. Our approximation which smoothes over the weak structure should not however be confused with the neglect of bending vibrations. The result obtained in the present study is a mean absorption cross section, on which the weak structure will be superimposed if the time evolution were indeed performed for long times instead of using the short time approximation in Appendix A.

4. Results and Discussion

[26] The normal mode frequencies for each of the isotopomers were obtained using the method described in Appendix B and are given in Table 1. The method of calculating the parameter α, as it appears in the N-O stretching wave function in section 3 and β, as it appears in the bending wave functions given in Table C1, is also given in Appendix C. α^2 and β^2 are defined there and their values for the various isotopomers are also given. These values were introduced into the wave functions for the further calculation.

[27] Using these values the calculated absorption cross section for 446 at 297 K is compared in Figure 1 with the experimental absorption cross sections of *Yoshino et al.* [1984] at 299 K, *von Hessberg et al.* [2004] at 283 K, and with the spectra calculated numerically from wave packet propagation by *Johnson et al.* [2001] at 300 K and by *Nanbu and Johnson* [2004] at 283 K. Our peak value in the absorption and its position that we obtained are 1.53×10^{-19} cm^2 and 53,600 cm^{-1}, as compared to the measured values of about 1.4×10^{-19} cm^2 and 55,000 cm^{-1}. In Figure 1, the peak was rescaled by a factor of 0.91 and shifted to the right by about 1400 cm^{-1} to make the comparison of the shape with the experimental measurement clearer. The shift arises from a small error in the difference between the energy of the ground and excited state electronic energies obtained from ab initio calculations. The total absorption cross sections for the 447, 448, 456 and 546 at 297 K were calculated similarly and the same shift in peak position, as for 446, was applied to all of these isotopomers. The peak position of the absorption cross sections of *Johnson et al.* [2001] and of *Nanbu and Johnson* [2004] are lower than that of the measured cross section by 1000 cm^{-1} and 1300 cm^{-1}. In Figure 1 alone, the peak obtained by *Johnson et al.* [2001] and *Nanbu and Johnson* [2004] was shifted by these amounts and rescaled to

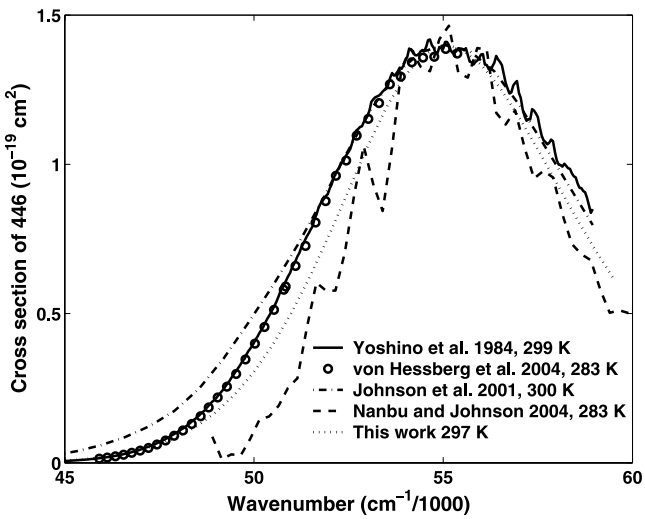

Figure 1. Absorption cross section of 446, peaks shifted and peak height rescaled for all three calculations.

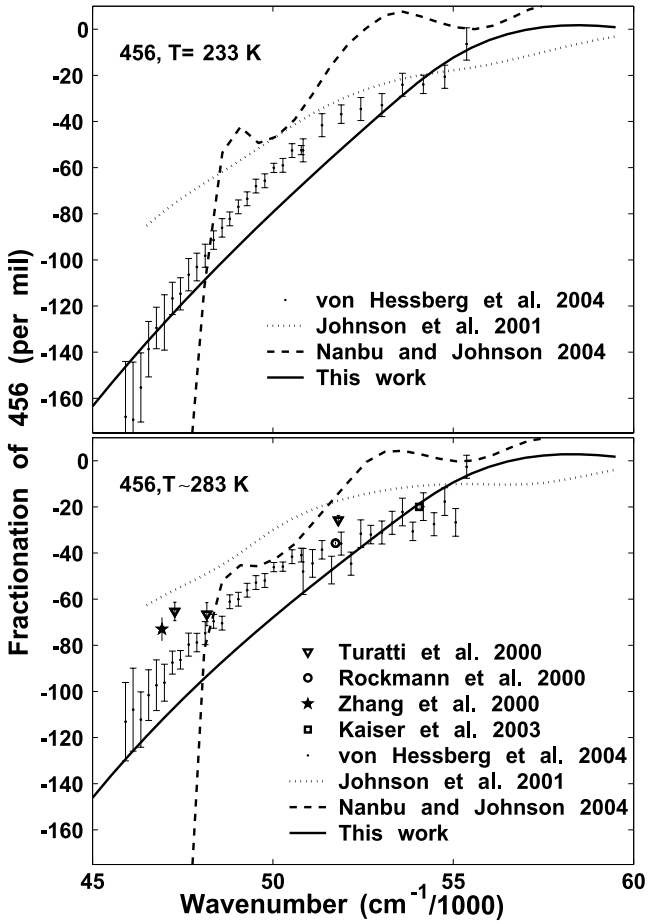

Figure 2. Fractionation of 456 at 233 K and 283 K.

facilitate the comparison. The results of the calculation are presented as a function of wave number rather than wavelength, since then any application of a peak shift does not distort the shape of the plot. According to *Hopper* [1984], the force constant for the N-N stretching in the excited electronic state is about 2.3 times less than that in the ground electronic state. When this value is used, we get the zero-point energy corresponding to N-N stretching in the excited electronic state to be less than that in the ground state by approximately $0.17\nu_3$ for a given isotopomer. This zero-point energy difference (ΔZPE) reduces the vertical transition energy by $0.17\nu_3$ and was used in the absorption cross-section calculations. Since we are adjusting the position of the peak of 446, it is the difference in the ΔZPE's of different isotopomers, and not the absolute value of ΔZPE, that effects the fractionation calculations. When a more accurate local ZPE of N_2 in the excited N_2O electronic state becomes available, the calculated spectra can be shifted by the difference from the value used here.

4.1. Wavelength-Dependent Fractionation

[28] The fractionations for the isotopomers relative to the most abundant isotopomer 446, calculated as described in the previous section, are given in Figures 2–6. Because of the weak structure it is possible that there could be substantial fluctuations in the local fractionation as a function of the wave number, perhaps reflected in the measurements in the form of error bars in fractionation. In the calculations, by neglecting the weak structure, we smooth over the fluctuations and so obtain the mean line for comparison with the mean line for the experiments. In application to atmospheric systems the breadth of the light source averages over fine structure. The results of the current calculation are compared in these figures with the experimental data of *Rockmann et al.* [2000, 2001a], *Turatti et al.* [2000], *Zhang et al.* [2000], and *Kaiser et al.* [2003] and the wide range of wavelength measurements of *von Hessberg et al.* [2004]. The results are also compared with the wave packet calculations of *Johnson et al.* [2001] and of *Nanbu and Johnson* [2004], without applying any shift of the peak position to their results. A comparison of the semiempirical calculations of *Yung and Miller* [1997], using the differences in zero-point energy (ZPE) of all the modes, by *Liang et al.* [2004], using the difference in ZPE of the two stretching modes, with some experimental measurements and also with the results of *Johnson et al.* [2001] has been given by *Liang et al.* [2004]. Only a comparison with the experiments and with the detailed theoretical calculations is given here.

[29] The sensitivity of the variation of the fractionations of the various isotopomers to changes in wave number of the absorption, in both experiment and our calculations, is $556 > 456 > 448 > 447 \sim 546$. The small variation of 546 and 447 relative to that in others reflects the fact that the

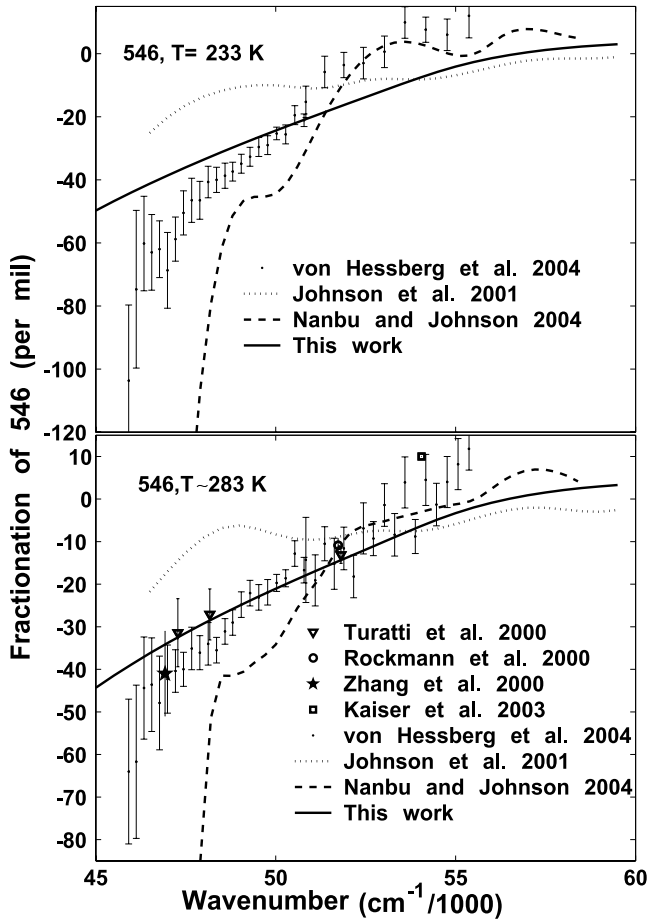

Figure 3. Fractionation of 546 at 233 K and 283 K.

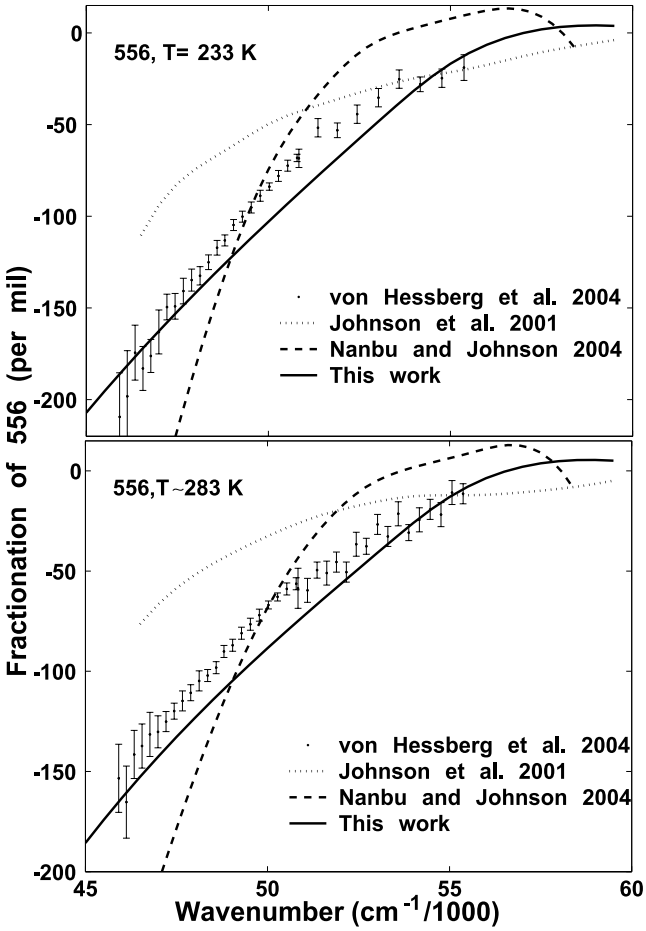

Figure 4. Fractionation of 556 at 233 K and 283 K.

normal mode frequencies for 546 and 447 differ very little from those of the 446 (Table 1). In most cases the present treatment yields improved results compared with the time-dependent treatments by *Johnson et al.* [2001] and *Nanbu and Johnson* [2004]. This improvement can be seen even if appropriate peak shifts were applied to these time-dependent cases, although that was not done in Figures 2–6 of this work. The present result and that of *Johnson et al.* [2001] show the maximum deviation for 546 at the longest wavelengths. The freezing of N-N bond was suspected to be the reason, but *Nanbu and Johnson*'s [2004] work, which included the N-N bond changes, as seen in Figures 2–4, yielded poorer results in this region. In another vein, zeroth-order correction to our fractionation calculations, made by matching the measured and calculated absorption frequencies at a given intensity of the absorption cross section is given in Appendix D. The correction is seen there to be small but to be closer to experiment.

[30] The absorption spectrum has contributions from the ground, first and the second bending vibrations, the higher "hot band" contributions occurring at higher temperatures. The transition dipole moment increases with the bending angle, and at the same time the vibrationally excited bending states in which high bending angles are possible have a lower thermal population. The contribution from different vibration modes is shown for 456 in Figure 7. At room temperature, the total fraction of first excited bending state, including the different initial state wave functions describing the degeneracy, is 10% and that of second excited state is less than 1%. However, at wavelengths longer than 200 nm, the excited bending modes contribute significantly to the fractionation, as seen from the "total" differing from the ground state alone fractionation by more than 30 per mil. It should be noted that the "total," indicated in the figure, is not the sum of the fractionations due to individual modes, but it is the fractionation calculated after summing the individual mode contributions to absorption cross section of 456 and dividing by that of 446. At some wave numbers, the "total" fractionation could be more positive than it is in each of the individual modes, because at a given temperature, the thermal population of the excited states in 456 is slightly more than that of 446 because of the different vibrational frequencies of the isotopomers, leading to a slightly higher photolysis cross section of 456.

[31] The laboratory fractionation studies of 447 and 448 by *Johnston et al.* [1995] were performed at 185 nm and this choice of wavelength resulted in near-zero fractionations of both 447 and 448. A later analysis [*Kaiser*, 2002] showed that for these values of measured fractionations the scatter was too large for a suitable fractionation line to be drawn, presumably because of the high noise in the near-zero fractionations [*Kaiser*, 2002]. So, no comparison with this data set was made.

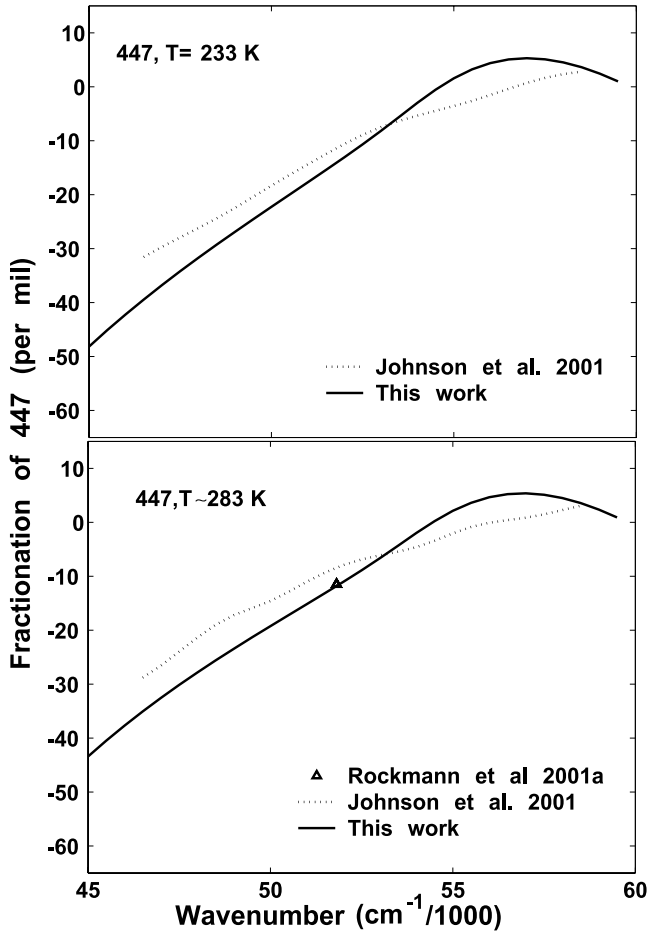

Figure 5. Fractionation of 447 at 233 K and 283 K.

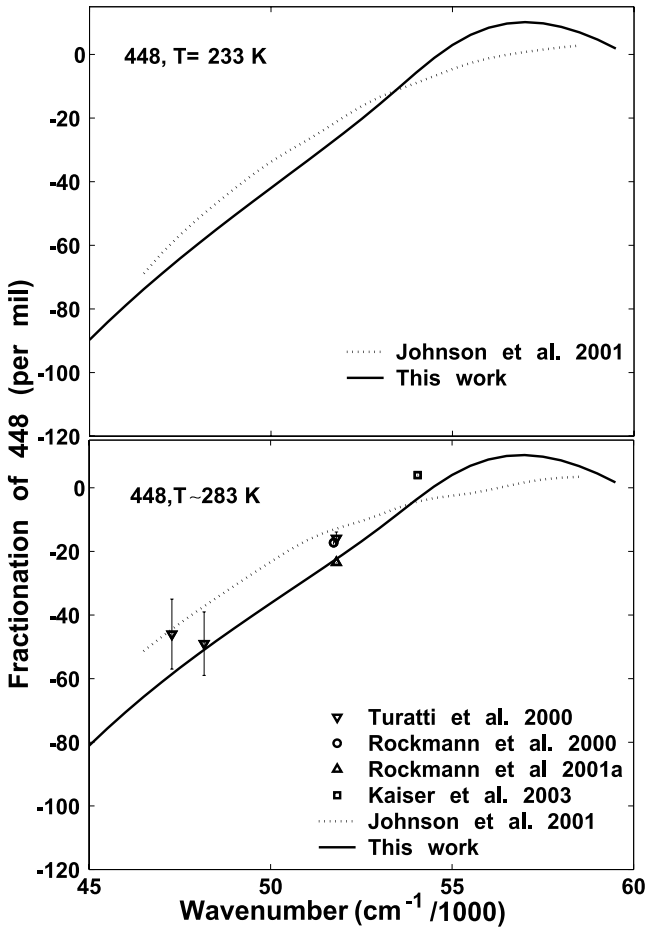

Figure 6. Fractionation of 448 at 233 K and 283 K.

[32] Before the results of *Daud et al.* [2005] were published, our calculations were based on the potential energy and dipole moment surfaces of *Brown et al.* [1999]. The results obtained with that are comparable to the ones reported in this paper, with the absorption cross section about 1.15 times the current value and the fractionations within a maximum of 20 per mil of the results reported here.

[33] To estimate the error in using a 1-D instead of 2-D bending wave functions, the total absorption cross section was calculated by summing the absorption cross section for each initial vibrational energy using 1-D harmonic oscillator wave functions, weighted by a degeneracy factor. The resulting cross section has the same shape as that obtained using 2-D bending wave functions. The peak intensity is about 2 times smaller and the peak position occurs at about 800 cm^{-1} higher than before. The fractionations calculated with the 1-D wave functions, after accounting for the appropriate peak shift, are approximately 20–25% different from those calculated with the 2-D bending wave functions. The difference between the two results for the case of 556 is illustrated in Figure 8. This difference is qualitatively the same for all the other isotopomers. After considering the shift in the absorption cross section that would be needed for *Johnson et al.* [2001], the 1-D wave function results at around 47,500 cm^{-1} account for about 70% of the difference between the calculations of *Johnson et al* [2001] and the measurements.

4.2. Broadband Calculations and Atmospheric Relevance

[34] In the above discussion, the results of our calculations were compared with the wavelength-dependent fractionation measurements. In the atmosphere, there is a flux of photons over a wide range of wavelengths, and the resultant fractionation occurs because of the simultaneous fractionation at all those wavelengths. Here we make a comparison with the broadband (185–225 nm) photolysis results of *Rockmann et al.* [2001b]. Using an antimony (Sb) lamp at room temperature, *Rockmann et al.* [2001b] obtained fractionations of -34.2 ± 0.8, -54 ± 1.6 and -21.9 ± 1.1 for ϵ^{448}, ϵ^{456} and ϵ^{546}, respectively. When a 207 nm filter was used on the lamp, there was no noticeable change in their experimental results. However, the fractionation constants compared with and without the filter differed by about 2 to 4 per mil in the later experiments of *Kaiser* [2002]. The wavelength-dependent fractionations that we obtained, av-

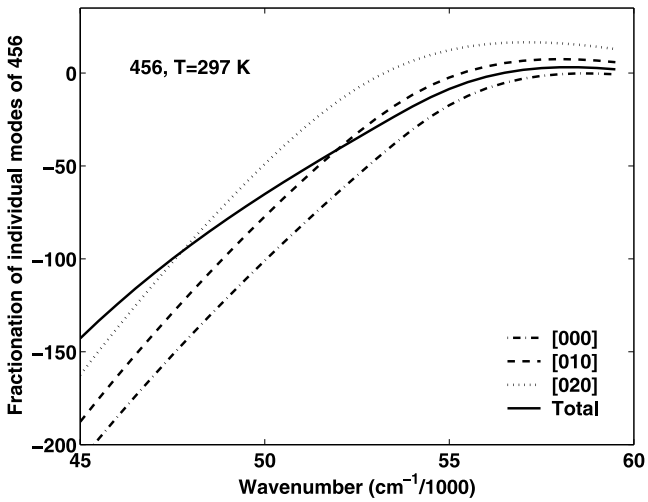

Figure 7. Contribution of various bending modes of 456 to the sum.

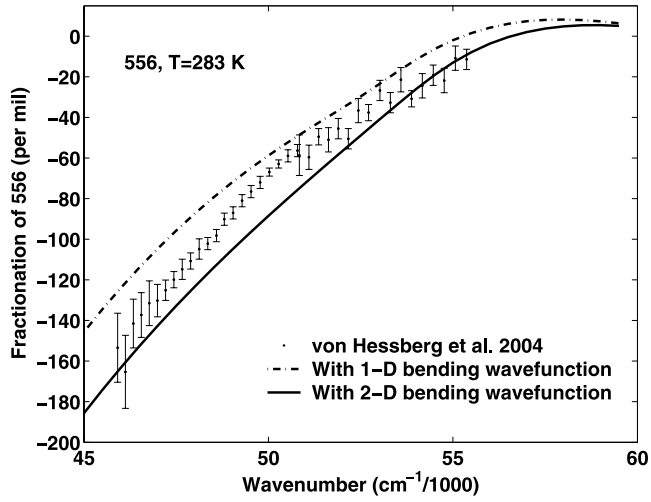

Figure 8. Fractionation of 556 at 283 K using 1-D and 2-D bending wave functions.

eraged using the relative overlap of the N_2O absorption and Sb emission spectrum [*Rockmann et al.*, 2001b, Plate 4] as the weighting factor, gives (ϵ^{447}, ϵ^{448}, ϵ^{456}, ϵ^{546}, ϵ^{556}) as (−19.2, −36.1, −68.0, −21.1, −88.4) and (−22.9, −43.1, −82.1, −25.2, −106.1) at 297 K and 233 K. With the 207 nm filter our results are (−23.7, −44.7, −82.3, −25.3, −106.4) and (−28.1, −52.8, −98.6, −30.1, −127.0) at 297 K and 233 K. The ratio of $\epsilon^{447}/\epsilon^{448}$ from our calculations in all the above cases is between 0.530 and 0.532. In a detailed analysis of the atmospheric relevance the results of the current calculation can be incorporated into a model which contains the transport of N_2O in the atmosphere [*McLinden et al.*, 2003; *Morgan et al.*, 2004], in addition to these photolysis results.

[35] A significant overlap of the N_2O absorption spectrum with the actinic fluxes in stratosphere exists in the wave number range 45,000 to 53,500 cm^{-1} [*Rockmann et al.*, 2001b, Plate 4]. For the wave numbers in this range, using the detailed calculations in the present work, the slope of the three-isotopic plot of $\ln(1 + \epsilon^{447})$ at each wave number, versus $\ln(1 + \epsilon^{448})$ at the same wave number is calculated to be 0.525.

[36] A perturbation theoretical expression for the slope of the three-isotope plot in the case of photolytic fractionation, obtained analytically with no computation, is given by *Prakash and Marcus* [2005]. The result obtained to first order in mass effects is the same as that obtained by *Bigeleisen and Mayer* [1947] for chemical equilibria [*Prakash and Marcus*, 2005]. The slope by perturbation analysis for $\ln(1 + \epsilon^{447})$ versus $\ln(1 + \epsilon^{448})$ plot is $(1/m_{O^{16}} - 1/m_{O^{17}})/(1/m_{O^{16}} - 1/m_{O^{18}}) = 0.529$.

[37] In virtue of the close agreement between the slope 0.525 obtained by detailed calculations and the slope obtained with no computation 0.529, we suggest that the slope for mass-dependent photolytic fractionation in a plot of $ln(1 + \epsilon^{447})$ versus $ln(1 + \epsilon^{448})$ is 0.525. In another form of presenting the fractionation, a ϵ^{447} versus ϵ^{448} plot, the slope with our detailed calculations is 0.532 [*Prakash and Marcus*, 2005]. A slope of 0.515 was obtained from an assortment of nonphotolytic thermal data [*Cliff and Thiemens*, 1997]. We suggest that a slope of ϵ^{447} versus ϵ^{448} plot differing from 0.532 for photolysis be considered an anomalous fractionation [*Prakash and Marcus*, 2005]. However, a small deviation from this slope is not as striking as the mass-independent fractionation found in O_3 formation [*Thiemens and Heidenreich*, 1983] governed by the symmetry effects [*Gao and Marcus*, 2002].

[38] The question of the contribution of photolytic fractionation to "anomalous" atmospheric observations [*Cliff et al.*, 1999] is previously discussed [*McLinden et al.*, 2003; *Kaiser et al.*, 2004, and references therein]. The result of the present work, in conjunction with a transport model, can be used to see what fraction of the enrichment of 447 in the stratosphere can be accounted for by photodissociation.

5. Conclusions

[39] In absorption cross sections of N_2O isotopomers calculated using a computationally simple time-independent multidimensional reflection principle, the cross section obtained for 446 is in good agreement with the broad envelope of the experimental cross section, with a shift in peak position. The fractionation of heavy isotopomers obtained in this relatively simple calculation as a function of the wavelength, after introducing this peak shift in all isotopomers correctly accounts for the observed fractionation of 448, 456, 546 and 556. The method does require potential energy and dipole moment surfaces obtained from ab initio calculations. Once the potential energy surfaces are obtained the calculation is not computationally intensive. Specific quantities of atmospheric relevance can be calculated by incorporating the results of the present work into a transport model.

Appendix A: Approximate Expression for the Absorption Cross Section

[40] Equation (4) gives a time-independent expression for the absorption cross section as:

$$\sigma_{i\nu}(\omega) = \frac{\pi}{\hbar\epsilon_0 c}\sum_{\nu'} \omega\, \delta\left(\omega_{f\nu',i\nu} - \omega\right)\, |\langle\Psi_{\nu'}|\mathbf{e}.\boldsymbol{\mu}_{fi}|\Psi_{\nu}\rangle|^2$$

This equation can be converted into a time-dependent form [*Schatz and Ratner*, 2002] using the identity:

$$\delta\left(\omega - \omega_{f\nu',i\nu}\right) = \frac{1}{2\pi}\int_{-\infty}^{\infty} e^{i\left(\omega-\omega_{f\nu',i\nu}\right)}dt \qquad \text{(A1)}$$

in the equation (4). Using another identity

$$e^{-iH_f t/\hbar} = \sum_{\nu'} |\Psi_{f\nu'}\rangle e^{-iE_{f\nu'}t/\hbar}\langle\Psi_{f\nu'}| \qquad \text{(A2)}$$

where H_f is the Hamiltonian of the excited state and $E_{f\nu'}$ the energy of the final vibronic state ($f\nu'$). $\sigma_{i\nu}$ can be rewritten as [*Schatz and Ratner*, 2002]:

$$\begin{aligned}\sigma_{i\nu} &= \frac{\pi\omega}{\hbar\epsilon_0 c}\frac{1}{2\pi}\int_{-\infty}^{\infty}\left(\langle\Psi_\nu|\ \mathbf{e}.\boldsymbol{\mu}_{fi}^{\dagger}\ e^{-iH_f t/\hbar}\ \mathbf{e}.\boldsymbol{\mu}_{fi}\ |\Psi_\nu\rangle\right)e^{i(\omega+E_{i\nu}/\hbar)t}\ dt \\ &= \frac{\pi\omega}{\hbar\epsilon_0 c}\frac{1}{2\pi}\int_{-\infty}^{\infty}(\langle y(0)|y(t)\rangle)e^{i(\omega+E_{i\nu}/\hbar)t}\ dt \qquad \text{(A3)}\end{aligned}$$

where $|y(t)\rangle = e^{-iH_f t/\hbar}|y(0)\rangle = e^{-iH_f t/\hbar}\mathbf{e}.\boldsymbol{\mu}_{fi}|\Psi_\nu\rangle$. In this form it is seen that $\sigma_{i\nu}$ is proportional to the Fourier transform of the autocorrelation function $\langle y(0)|y(t)\rangle$.

[41] The time-dependent approach involves finding the time-evolution of the autocorrelation function under the Hamiltonian H_f and then its Fourier transform. To obtain a simpler form in the time-independent approach, an approximation is made, shown to be valid to first order in time t [*Lee et al.*, 1983], that at short times of evolution the operator H_f can be replaced by $\langle T\rangle_{i\nu}^{(\mu)} + V_f$, where V_f is the potential energy operator of the excited state. T is kinetic energy operator, which is the same in ground and excited electronic states and $\langle T\rangle_{i\nu}^{(\mu)} = \langle\Psi_{i\nu}\ |\mathbf{e}.\boldsymbol{\mu}_{fi}^{\dagger}\ T\ \mathbf{e}.\boldsymbol{\mu}_{fi}|\Psi_{i\nu}\rangle/\langle\Psi_{i\nu}\ |\mathbf{e}.\boldsymbol{\mu}_{fi}^{\dagger}\ \mathbf{e}.\boldsymbol{\mu}_{fi}|\Psi_{i\nu}\rangle$. The averaged kinetic energy $\langle T\rangle_{i\nu} = \langle\Psi_{i\nu}|T|\Psi_{i\nu}\rangle/\langle\Psi_{i\nu}|\Psi_{i\nu}\rangle$ of the vibrational state ν in the ground electronic state i, equal to $(1/2)E_{i\nu}$ for a harmonic approximation to the potential energy [*Lee et al.*, 1983] and we found by calculation that it differs from $\langle T\rangle_{i\nu}^{(\mu)}$ by only about 10 cm^{-1}. This spectral shift is negligible. So in the present work $\langle T\rangle_{i\nu}^{(\mu)}$ is approximated by $(1/2)E_{i\nu}$.

[42] Physically, the meaning in the time-dependent picture is that because of the excitation, the wave packet from the ground electronic state is promoted to the excited electronic surface instantaneously and the dynamics of the autocorrelation is considered as the wave packet evolves under excited state Hamiltonian. Since $\sigma_{i\nu}$ is given by the Fourier transform of the autocorrelation function in equation (12), the present short time approximation for the time evolution has as a consequence that one can only obtain the broad features of the absorption cross section (the envelope) rather than its fine structure. The method is well suited to the analysis of direct or nearly direct dissociation problems, where the lifetime of the wave packet is small in the excited electronic state and the superimposed structure is not dominant over the broad background of the absorption. Using the identity in equation (10), the absorption cross section is converted back into the time-independent form using the short time approximation given by *Lee et al.* [1983]:

$$\sigma_{i\nu} = \frac{\pi\omega}{\hbar\epsilon_0 c}\langle\Psi_\nu|\ \mathbf{e}.\boldsymbol{\mu}_{fi}^{\dagger}\ \delta\left(\omega - \left(V_f + \langle T\rangle_{i\nu} - E_{i\nu}\right)/\hbar\right)\ \mathbf{e}.\boldsymbol{\mu}_{fi}\ |\Psi_\nu\rangle$$
$$= \frac{\pi\omega}{\hbar\epsilon_0 c}\int |\Psi_\nu(\mathbf{Q})|^2 \left|\mathbf{e}.\boldsymbol{\mu}_{fi}(\mathbf{R})\right|^2 \delta\left(\omega - \left(V_f - \frac{1}{2}E_{i\nu}\right)/\hbar\right) d\mathbf{R} \tag{A4}$$

where the second line in the equation above is a coordinate representation of the first line. The dipole moment function $\boldsymbol{\mu}_{fi}(\mathbf{R})$ is obtained by ab initio calculations. Averaging over all possible directions, **e**, of the electric field, we get the absorption cross section by replacing $|\mathbf{e}.\boldsymbol{\mu}_{fi}|^2$ with (1/3) $|\mu_{fi}|^2$, μ_{fi} being the magnitude of the vector $\boldsymbol{\mu}_{fi}$.

$$\sigma_{i\nu} = \frac{\pi\omega}{3\hbar\epsilon_0 c}\int |\Psi_\nu(\mathbf{R})|^2 \left|\mu_{fi}(\mathbf{R})\right|^2 \delta\left(\omega - \left(V_f - \frac{1}{2}E_{i\nu}\right)/\hbar\right) d\mathbf{R} \tag{A5}$$

Appendix B: Normal Mode Calculation

[43] The procedure for finding the normal modes of vibration and the normal coordinates in terms of the internal coordinates is described by *Califano* [1976] and *Steele* [1971]. The inertia matrix G^{-1}, which has the details of the masses and moments of inertia of the molecule, and the force constant matrix F are used for this transformation. We denote the deviations of the internal coordinates from the equilibrium values (r_{NN}^{eq}, r_{NO}^{eq}, θ^{eq}) by (r_{NN}, r_{NO}, θ). The inertia matrix G for the linear molecule N_2O is defined by *Califano* [1976] ($G_{\theta\theta}$, not discussed by Califano, is given by *Ferigle and Meister* [1951]).

$$G = \begin{pmatrix} \mu_1+\mu_2 & \mu_2 & 0 \\ \mu_2 & \mu_2+\mu_3 & 0 \\ 0 & 0 & \frac{\mu_1}{\left(r_{NN}^{eq}\right)^2} + \frac{\mu_3}{\left(r_{NO}^{eq}\right)^2} + \mu_2\left(\frac{1}{\left(r_{NN}^{eq}\right)} + \frac{1}{\left(r_{NO}^{eq}\right)}\right)^2 \end{pmatrix} \tag{B1}$$

where $\mu_i = 1/m_i$, m_i being the mass of the atom in the ith position ($N^{(1)}$-$N^{(2)}$-$O^{(3)}$).

[44] The potential and kinetic energy expressions in the matrix form are: $2V = R^T F R$ and $2T = P^T G P$, where R is a column matrix whose rows R_1, R_2 and R_3 are r_{NN}, r_{NO} and θ, and P is the momentum matrix conjugate to R. Using Hamilton's equation, we have $\dot{R} = \partial T/\partial P = GP$. Using this relation and the symmetry of G (namely that its transpose, G^T, equals itself, G), $2T = \dot{R}^T(G^{-1})^T\ GG^{-1}\ \dot{R} = \dot{R}^T G^{-1}\ \dot{R}$. The normal coordinates Q are transformed in terms of the internal coordinates R. Using a linear transformation L from Q to R, $R = LX$ the expressions for the kinetic and potential energies can be rewritten as: $2\ V = Q^T L^T F L Q$ and $2T = \dot{Q}^T L^T G^{-1} L \dot{Q}$. To reduce these into the standard forms for normal coordinates, we use the conditions: (1) $L^T G^{-1} L$ and $L^T F L$ are diagonal. This transformation can be achieved by forming L from the eigenvectors of the GF matrix. Then, L simultaneously diagonalizes F and G^{-1}. (2) Comparison with the standard form of normal coordinate kinetic energy gives $L^T G^{-1} L = I$ and removes the arbitrary scaling factors in the eigenvectors that form L, thus making the transformation $R = LQ$ unique.

[45] The natural frequencies for the normal modes are calculated using $\frac{1}{2}\dot{Q}^T L^T G^{-1} L \dot{Q} - L^T F L = 0$, i.e., $W - L^T F L = 0$, where W is a diagonal matrix with elements $W_{i,i} = \omega_i^2$. In conformity with the standard notation, we choose the order of ω_i's such that ω_2 corresponds to the bending vibration and ω_1 and ω_3 to the stretching vibrations. The ω_i's are related to the ν_i's in Table 1 as $\omega_i = 2\pi\nu_i$ The data required for the calculation of G matrix are: atomic masses of isotopes in amu → ^{14}N - 14.0; ^{15}N - 15.0; ^{16}O - 16.0; ^{18}O - 18.0; equilibrium bond lengths → r_{NN}^{eq} = 1.1273 A; r_{NO}^{eq} = 1.1851 A.

Appendix C: Calculation of α and β

[46] In the ground vibrational state, the amplitude of the wave function is given in terms of the normal coordinates as: $|\Psi|^2 \propto \exp(-\Sigma\omega_i Q_i^2/\hbar)$, where Q_i are the elements of the normal coordinate matrix Q, defined in the previous section. Converting these normal coordinates into internal displacement coordinates, R_i and leaving the normalization factor that includes the Jacobian of the transformation, we have:

$$|\Psi|^2 \propto \exp\left(-\Sigma\omega_i\left(L_{ij}^{-1}R_j\right)^2/\hbar\right)$$
$$= \exp\left(-A_1 r_{NN}^2 - A_2 r_{NO}^2 - 2A_3 r_{NN} r_{NO} - A_4\theta^2\right)$$
$$\propto \exp\left(-A_1(r_{NN} + A_3/A_1 r_{NO})^2 - \left(A_1A_2 - A_3^2\right)r_{NO}^2/A_1 - A_4\theta^2\right) \tag{C1}$$

where L_{ij}^{-1} are the elements of the inverse of the matrix L defined in the previous section, R_j are the internal displacement coordinates r_{NN}, r_{NO} and θ. The coefficients A_is were obtained in terms of ω, L_{ij}^{-1} and $\hbar$, by the rearrangement of the internal coordinate terms in equation (15): $A_1 = 1/\hbar\ (\omega_1\ (L_{11}^{-1})^2 + \omega_3\ (L_{31}^{-1})^2)$, $A_2 = 1/\hbar\ (\omega_1\ (L_{13}^{-1})^2 + \omega_3\ (L_{33}^{-1})^2)$, $A_3 = 1/\hbar\ (\omega_1\ (L_{11}^{-1}\ L_{13}^{-1}) + \omega_3\ (L_{31}^{-1}\ L_{33}^{-1}))$ and $A_4 = 1/\hbar\ (\omega_2\ (L_{22}^{-1})^2)$.

[47] Defining $(r_{NN} + A_3/A_1 r_{NO})$ and r_{NN} as the two independent coordinates, the former is seen to be irrelevant for the absorption analysis since the potentials and dipole moments are independent of that coordinate. In the expression for the absorption cross section, the term corresponding to this coordinate would thus on integration, yield unity. Comparing the coefficient of θ^2 with that for the ground

state wave function in Table C1 in Appendix C, we obtain the parameter $\beta^2 = A_4$. Similarly, α^2 is $(A_1A_2 - A_3^2)/A_1$.

[48] In this paper, we use the force constant data F for N_2O available from *Csaszar* [1994] and obtained by their fit to the experimental data on vibration frequencies. These force constants in the units of aJ/A^2 are as follows: $F_{r_{NN}r_{NN}}$, 18.251; $F_{r_{NO}r_{NO}}$, 11.960; $F_{r_{NN}r_{NO}}$, 1.028; $F_{\theta\theta}$, 0.666; $F_{r_{NN}\theta}$, 0; $F_{r_{NO}\theta}$, $F_{r_{NO}\theta}$, 0.

[49] The values of (α^2, β^2) thus obtained, in units of (10^4/nm^2, /rad^2) are (3.7847, 55.9644), (3.8457, 56.1997), (3.9023, 56.4105), (3.8418, 57.2736), (3.7881, 56.2995) and (3.8450, 57.6329) for 466, 447, 448, 456, 546 and 556 isotopomers.

Appendix D: Zeroth-Order Correction to the Calculations

[50] In Figure 1, we see that the absorption cross section calculated in this work, based on vibronic transitions alone, is slightly narrower than the measured absorption cross section. There can be a broadening in this absorption cross section if we also include the contribution of the transitions between the rotational states, say J to $J + 1$, with thermal populations that depend upon the energies of the states, $E_J = BJ(J + 1)$ and $E_{J+1} = B(J + 1)(J + 2)$. Here, B is the rotational constant. For such a case, corresponding to a total absorption frequency, the vibronic transition will happen at a frequency less by the energy difference $\Delta E = E_{J+1} - E_J = 2B(J + 1)$. The total absorption cross section would be obtained as the sum of the vibronic cross sections, shifted by the rotational excitation and weighted by the thermal probability of being in the rotational state J. With the total cross section given by the convolution of the thermal probability distribution as a function of the ΔE and the vibronic cross section, if we approximate both of these by Gaussian distributions with variances s_{vib}^2 and s_{rot}^2, the variance of the total absorption cross section will be $s_{vib}^2 + s_{rot}^2$. Since in the case of N_2O, $s_{vib} \sim 2750$ cm^{-1} and $s_{rot} \sim 10$ cm^{-1}, the effect of the inclusion of the rotation on the width of the total absorption cross section is negligible. Including the other branches $\Delta J = 0, -1$ also has a negligible effect on the width.

[51] It is assumed that the difference between the measured and the calculated cross sections were due to the potential energy surfaces as one of at least two possibilities, a zeroth-order correction to our calculation of fractionation calculations can be made as follows. To implement this correction, after rescaling the height and shifting the peak of the calculated cross section, corresponding to an intensity in the calculated cross section, the actual absorption wave number (ω_{meas}), which is slightly higher or lower than the calculated one (ω_{calc}) is noted. Then the fractionations calculated as a function of ω_{calc} are plotted as functions of ω_{meas} instead. This new plot is illustrated for the case of 556 isotopomer in Figure D1. The difference in the fractionation obtained by such a correction is small, but noticeable in the scale of the plots. This correction would be applicable to calculations at temperatures ~283 K or 233 K, for which we know the absorption cross section [*Yoshino et al.*, 1984; *von Hessberg et al.*, 2004].

Table C1. Wave Functions for Doubly Degenerate Bending Vibration

n	m	Wave Function
0	0	$\frac{\beta}{\sqrt{\pi}} e^{-\beta^2\theta^2/2}$
1	1	$\frac{\beta}{\sqrt{\pi}} \beta\theta\, e^{-\beta^2\theta^2/2}\, e^{i\phi}$
1	−1	$\frac{\beta}{\sqrt{\pi}} \beta\theta\, e^{-\beta^2\theta^2/2}\, e^{-i\phi}$
2	2	$\frac{\beta}{\sqrt{2\pi}} (\beta\theta)^2\, e^{-\beta^2\theta^2/2}\, e^{2\,i\phi}$
2	0	$\frac{\beta}{\sqrt{\pi}} [(\beta\theta)^2 - 1] e^{-\beta^2\theta^2/2}$
2	−2	$\frac{\beta}{\sqrt{2\pi}} (\beta\theta)^2\, e^{-\beta^2\theta^2/2}\, e^{2i\phi}$

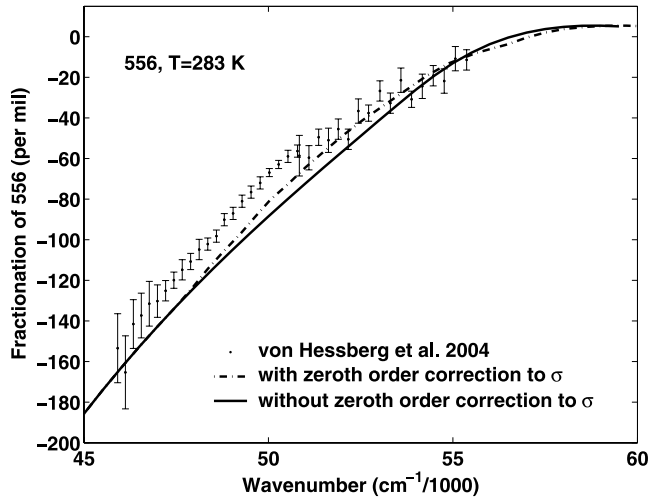

Figure D1. Fractionation of 556 at 283 K with and without the zeroth-order correction to the absorption cross section described in Appendix D.

[52] **Acknowledgments.** It is a pleasure to acknowledge the support of this research by the National Science Foundation. We would like to particularly thank G. G. Balint-Kurti for immediately providing us with the results of their calculations on N_2O potential energy surfaces. We thank Wei-Chen Chen for all the valuable discussions and his tutelage (of M.K.P.) in chemical concepts. We also thank M. C. Liang, G. A. Blake, and Y. L. Yung for sharing with us the results of their work before publication. We are indebted to Matt Johnson for his very helpful comments.

References

Amiot, C. (1976), Vibration-rotation bands of $^{15}N_2^{16}O$-$^{14}N_2^{18}O$, *J. Mol. Spectrosc.*, *59*, 380–395.

Atkinson, R., D. L. Baulch, R. A. Cox, R. F. Hampson Jr., J. A. Kerr, M. J. Rossi, and J. Troe (1997), Evaluated kinetic, photochemical and heterogeneous data for atmospheric chemistry: Supplement V. IUPAC Subcommittee on Gas Kinetic Data Evaluation for Atmospheric Chemistry, *J. Phys. Chem. Ref. Data*, *26*, 521–1011.

Bigeleisen, J., and M. G. Mayer (1947), Calculation of equilibrium constants for isotopic exchange reactions, *J. Chem. Phys.*, *15*(5), 261–267.

Blake, G. A., M. C. Liang, C. G. Morgan, and Y. L. Yung (2003), A Born-Oppenheimer photolysis model of N_2O fractionation, *Geophys. Res. Lett.*, *30*(12), 1656, doi:10.1029/2003GL016932.

Brenninkmeijer, C. A. M., C. Janssen, J. Kaiser, T. Rockmann, T. S. Rhee, and S. S. Assonov (2003), Isotope effects in the chemistry of atmospheric trace compounds, *Chem. Rev.*, *103*(12), 5125–5162.

Brown, A., P. Jimeno, and G. G. Balint-Kurti (1999), Photodissociation of N_2O: I. Ab initio potential energy surfaces for the low-lying electronic states $\tilde{X}$ 1A′, 2^1A′, and 1^1A″, *J. Phys. Chem. A*, *103*(50), 11,089–11,095.

Califano, S. (1976), *Vibrational States*, John Wiley, Hoboken, N. J.

Cliff, S. S., and M. H. Thiemens (1997), The $^{18}O/^{16}O$ and $^{17}O/^{16}O$ ratios in the atmospheric nitrous oxide: A mass-independent anomaly, *Science*, *278*, 1774–1776.

Cliff, S. S., C. A. M. Brenninkmeijer, and M. H. Thiemens (1999), First measurements of the $^{18}O/^{16}O$ and $^{17}O/^{16}O$ ratios in the stratospheric nitrous oxide: A mass-independent anomaly, *J. Geophys. Res.*, *104*, 16,171–16,175.

Cohen-Tannoudji, C., B. Diu, and F. Laloe (1977), *Quantum Mechanics*, vol. 1, John Wiley, Hoboken, N. J.

Csaszar, A. G. (1994), Anharmonic force field of N_2O, *J. Phys. Chem.*, *98*, 8823–8826.

Daud, M. N., G. G. Balint-Kurti, and A. Brown (2005), Ab initio potential energy surfaces, total absorption cross sections, and product quantum state distributions for the low-lying electronic states of N_2O, *J. Chem. Phys.*, *122*, 054305. (Potential energy and dipole moment surfaces are available at ftp://ftp.aip.org/epaps/journ_chem_phys/E-JCPSA6-122-303502/.)

Ferigle, S. M., and A. G. Meister (1951), Kinetic energy matrix elements for linear molecules, *J. Chem. Phys.*, *19*, 982–983.

Freed, K. F., and Y. B. Band (1977), Product energy distributions in the dissociation of polyatomic molecules, in *Excited States*, vol. 3, edited by E. C. Lim, pp. 109–201, Elsevier, New York.

Gao, Y. Q., and R. A. Marcus (2002), On the theory of strange and unconventional isotopic effects on ozone formation, *J. Chem. Phys.*, *116*, 137–154.

Hanisco, T. F., and A. C. Kummel (1993), State-resolved photodissociation of N_2O, *J. Phys. Chem.*, *97*, 7242–7246.

Heller, E. J. (1978), Quantum corrections to classical photodissociation models, *J. Chem. Phys.*, *68*(5), 2066–2075.

Herzberg, G. (1950), *Molecular Spectra and Molecular Structure: 1. Spectra of Diatomic Molecules*, pp. 391–394, D. Van Nostrand, Princeton, N. J.

Hopper, D. G. (1984), Ab initio multiple root optimization MCSCF study of the $C_{\infty v}/C_s$ excitation spectra and potential energy surfaces of N_2O, *J. Chem. Phys.*, *80*(9), 4290–4316.

Johnson, M. S., G. D. Billing, A. Gruodis, and M. H. M. Janssen (2001), Photolysis of nitrous oxide isotopomers studied by time-dependent Hermite propagation, *J. Phys. Chem. A*, *105*(38), 8672–8680.

Johnston, J. C., S. S. Cliff, and M. H. Thiemens (1995), Measurement of multioxygen isotopic ($\delta^{18}O$ and $\delta^{17}O$) fractionation factors in the stratospheric sink reactions of nitrous oxide, *J. Geophys. Res.*, *100*(D8), 16,801–16,804.

Jolma, K., J. Kauppinen, and V.-M. Horneman (1983), Vibration-rotation spectrum of N_2 in the region of the lowest fundamental ν_2, *J. Mol. Spectrosc.*, *101*, 278–284.

Kaiser, J. (2002), Stable isotope investigations of atmospheric nitrous oxide, Ph.D thesis, Johannes Gutenberg-Univ., Mainz, Germany.

Kaiser, J., T. Rockmann, C. A. M. Brenninkmeijer, and P. J. Crutzen (2003), Wavelength dependence of isotope fractionation in N_2O photolysis, *Atmos. Chem. Phys.*, *3*, 303–313.

Kaiser, J., T. Rockmann, and C. A. M. Brenninkmeijer (2004), Contribution of mass-dependent fractionation to the oxygen isotope anomaly of atmospheric nitrous oxide, *J. Geophys. Res.*, *109*(D3), D03306, doi:10.1029/2003JD003739.

Kim, K.-R., and H. Craig (1993), Nitrogen-15 and oxygen-18 characteristics of nitrous oxide: A global perspective, *Science*, *262*, 1855–1857.

Lee, S. Y. (1982), Semi-classical theory of radiation interacting with a molecule, *J. Chem. Phys.*, *76*, 3064–3074.

Lee, S. Y., R. C. Brown, and E. J. Heller (1983), Multidimensional reflection approximation: Application to the photodissociation of polyatomics, *J. Phys. Chem.*, *87*(12), 2045–2053.

Liang, M. C., G. A. Blake, and Y. L. Yung (2004), A semianalytic model for photo-induced isotopic fractionation in simple molecules, *J. Geophys. Res.*, *109*(D10), D10308, doi:10.1029/2004JD004539.

McLinden, C. A., M. J. Prather, and M. S. Johnson (2003), Global modeling of the isotopic analogues of N_2O: Stratospheric distributions, budgets, and the ^{17}O-^{18}O mass-independent anomaly, *J. Geophys. Res.*, *108*(D8), 4233, doi:10.1029/2002JD002560.

Minschwaner, K., R. J. Salawitch, and M. B. McElroy (1993), Absorption of solar-radiation by O_2: Implications for O_3 and lifetimes of N_2O, $CFCl_3$, and CF_2Cl_2, *J. Geophys. Res.*, *98*(D6), 10,543–10,561.

Morgan, C. G., M. Allen, M. C. Liang, R. L. Shia, G. A. Blake, and Y. L. Yung (2004), Isotopic fractionation of nitrous oxide in the stratosphere: Comparison between model and observations, *J. Geophys. Res.*, *109*(D4), D04305, doi:10.1029/2003JD003402.

Nanbu, S., and M. S. Johnson (2004), Analysis of the ultraviolet absorption cross sections of six isotopically substituted nitrous oxide species using 3D wave packet propagation, *J. Phys. Chem. A*, *108*(41), 8905–8913.

Naqvi, S. W. A., T. Yoshinari, D. A. Jayakumar, M. A. Altabet, P. V. Narvekar, A. H. Devol, J. A. Brandes, and L. A. Codispoti (1998), Budgetary and biogeochemical implications of N_2O isotope signatures in the Arabian Sea, *Nature*, *394*(6692), 462–464.

Nishida, S., K. Takahashi, Y. Matsumi, N. Taniguchi, and S. Hayashida (2004), Formation of $O(^3P)$ atoms in the photolysis of N_2O at 193 nm and $O(^3P) + N_2O$ product channel in the reaction of $O(^1D) + N_2O$, *J. Phys. Chem. A*, *108*(13), 2451–2456.

Park, S. Y., E. L. Atlas, and K. A. Boering (2004), Measurements of N_2O isotopologues in the stratosphere: Influence of transport on the apparent enrichment factors and the isotopologue fluxes to the troposphere, *J. Geophys. Res.*, *109*(D1), D01305, doi:10.1029/2003JD003731.

Prakash, M. K., and R. A. Marcus (2005), Three-isotope plot of fractionation in photolysis: A perturbation theoretical expression, *J. Chem. Phys. 123*, 174308.

Prasad, S. S. (1997), Potential atmospheric sources and sinks of nitrous oxide: 2. Possibilities from excited O_2, "embryonic" O_3, and optically pumped excited O_3, *J. Geophys. Res.*, *102*(D17), 21,527–21,536.

Preston, K. F., and R. F. Barr (1971), Primary processes in the photolysis of nitrous oxide, *J. Chem. Phys.*, *54*(8), 3347–3348.

Rahn, T., and M. Wahlen (1997), Stable isotope enrichment in stratospheric nitrous oxide, *Science*, *278*, 1776–1777.

Rockmann, T., C. A. M. Brenninkmeijer, M. Wollenhaupt, J. N. Crowley, and P. J. Crutzen (2000), Measurement of the isotopic fractionation of $^{15}N^{14}N^{16}O$, $^{14}N^{15}N^{16}O$ and $^{14}N^{14}N^{18}O$, *Geophys. Res. Lett.*, *27*(9), 1399–1402.

Rockmann, T., J. Kaiser, J. N. Crowley, C. A. M. Brenninkmeijer, and P. J. Crutzen (2001a), The origin of the anomalous or "mass-independent" oxygen isotope fractionation in tropospheric N_2O, *Geophys. Res. Lett.*, *28*(3), 503–506.

Rockmann, T., J. Kaiser, C. A. M. Brenninkmeijer, J. N. Crowley, R. Borchers, W. A. Brand, and P. J. Crutzen (2001b), Isotopic enrichment of nitrous oxide ($^{15}N^{14}NO$, $^{14}N^{15}NO$, $^{14}N^{14}N^{18}O$) in the stratosphere and in the laboratory, *J. Geophys. Res.*, *106*(D10), 10,403–10,410.

Schatz, G. C., and M. A. Ratner (2002), *Quantum Mechanics in Chemistry*, 201 pp., Dover, Mineola, N. Y.

Schinke, R. (1993), *Photodissociation Dynamics*, Cambridge Univ. Press, New York.

Selwyn, G. S., and H. S. Johnston (1981), Ultraviolet absorption spectrum of nitrous oxide as function of temperature and isotopic substitution, *J. Chem. Phys*, *74*, 3791–3803.

Steele, D. (1971), *Theory of Vibrational Spectroscopy*, W. B. Saunders, Philadelphia, Pa.

Stevens, C. M., D. Walling, A. Venters, L. E. Ross, A. Engelkem, and L. Krout (1972), Isotopic composition of atmospheric carbon-monoxide, *Earth Planet. Sci. Lett.*, *16*, 147–165.

Thiemens, M. H., and J. E. Heidenreich (1983), The mass-independent fractionation of oxygen: A novel isotope effect and its possible cosmochemical implications, *Science*, *219*, 1073–1075.

Toth, R. A. (1986), Frequencies of N_2O in the 1100 cm^{-1} to 1440 cm^{-1} region, *J. Opt. Soc. Am. B*, *3*, 1263–1281.

Toth, R. A. (1987), N_2O vibration-rotation parameters derived from measurements in the 900–1090 cm^{-1} and 1580–2380 cm^{-1} regions, *J. Opt. Soc. Am. B*, *4*, 357–374.

Turatti, F., D. W. T. Griffith, S. R. Wilson, M. B. Esler, T. Rahn, H. Zhang, and G. A. Blake (2000), Positionally dependent ^{15}N fractionation factors in the UV photolysis of N_2O determined by high resolution FTIR spectroscopy, *Geophys. Res. Lett.*, *27*(16), 2489–2492.

von Hessberg, P., J. Kaiser, M. B. Enghoff, C. A. McLinden, S. I. Sorensen, T. Rockmann, and M. S. Johnson (2004), Ultra-violet absorption cross sections of isotopically substituted nitrous oxide species: $^{14}N^{14}NO$, $^{15}N^{14}NO$, $^{14}N^{15}NO$, and $^{15}N^{15}NO$, *Atmos. Chem. Phys.*, *4*, 1237–1253.

Winans, J. G., and E. C. G. Stueckelberg (1928), The origin of the continuous spectrum of the hydrogen molecule, *Proc. Natl. Acad. Sci. U. S. A.*, *14*, 867–871.

Yoshino, K., D. E. Freeman, and W. H. Parkinson (1984), High-resolution absorption cross-section measurements of N_2O at 295 K-299 K in the wavelength region 170–222 nm, *Planet. Space Sci.*, *32*(10), 1219–1222.

Yung, Y. L., and C. E. Miller (1997), Isotopic fractionation of stratospheric nitrous oxide, *Science*, *278*, 1778–1780.

Yung, Y. L., W. C. Wang, and A. A. Lacis (1976), Greenhouse effect due to atmospheric nitrous-oxide, *Geophys. Res. Lett.*, *3*, 619–621.

Zhang, H., P. O. Wennberg, V. H. Wu, and G. A. Blake (2000), Fractionation of $^{14}N^{15}N^{16}O$ and $^{15}N^{14}N^{16}O$ during photolysis at 213 nm, *Geophys. Res. Lett.*, *27*, 2481–2484.

R. A. Marcus and M. K. Prakash, Noyes Laboratory of Chemical Physics, California Institute of Technology, MC 127-72, 1200 East California Boulevard, Pasadena, CA 91125, USA. (ram@caltech.edu; meher@caltech.edu)

J. D. Weibel, Division of Geological and Planetary Sciences, California Institute of Technology, MC 150-21, 1200 East California Boulevard, Pasadena, CA 91125, USA. (weibel@caltech.edu)